International Journal of Hydrogen Energy 116 (2025) 507–515

Contents lists available at ScienceDirect

International Journal of Hydrogen Energy

journal homepage: www.elsevier.com/locate/he

Heat capacity and other thermodynamic properties of *hcp*-CrH and *hcp*-CrD

Mikhail A. Kuzovnikov [a,*], Vladimir E. Antonov [b], Valery I. Kulakov [b], Radion I. Usmanov [b,c]

[a] Centre for Science at Extreme Conditions and School of Physics and Astronomy, University of Edinburgh, Edinburgh, EH9 3FD, United Kingdom
[b] Institute of Solid State Physics RAS, Moscow District, 142432, Chernogolovka, Russia
[c] National Research University Higher School of Economics, 20 Myasnitskaya Ul., 101000, Moscow, Russia

ARTICLE INFO

Handling Editor: C O Colpan

Keywords:
High hydrogen pressures
Chromium hydride and deuteride
Heat capacity
Phase diagram Cr–H

ABSTRACT

Polycrystalline samples of chromium hydride CrH and deuteride CrD with a hexagonal close-packed (*hcp*) metal lattice were synthesized at a hydrogen (deuterium) pressure of 7.4 GPa and a temperature of 873 K, rapidly cooled to 100 K, recovered to ambient pressure and studied by differential scanning calorimetry at temperatures from 120 to 220–240 K. The calorimetric study and density functional theory calculations helped to determine the isobaric heat capacity C_P of *hcp*-CrH at temperatures up to 1000 K and to clarify the shape and position of its acoustic phonon band and the coefficient of electronic heat capacity. The investigation of *hcp*-CrD demonstrated the approximately harmonic change in the energy of its optical vibrations compared with *hcp*-CrH. Using the obtained $C_P(T)$ dependence of *hcp*-CrH for the calculation of its Gibbs energy gave the line of the Cr + (1/2) H_2═CrH equilibrium in the *T-P* diagram of the Cr–H system. The position of this line corroborated the debatable opinion that the pressure of thermodynamic equilibrium is much closer to the pressure of hydride decomposition than to the pressure of its formation.

1. Introduction

Chromium hydride CrH with a hexagonal close-packed (*hcp*) metal lattice belongs to a fairly large group of hydrides of *d*-metals of groups VI–X of the Periodic Table, which are thermodynamically stable only at high hydrogen pressures (see Refs. [1,2]) and quickly decompose into metal and hydrogen gas under normal conditions. The lattice dynamics of most hydrides synthesized at pressures up to 9 GPa have previously been studied by inelastic neutron scattering (INS). The measured INS spectra, supplemented by *ab initio* calculations, were used to construct the $g(E)$ spectra of the phonon density of states of these hydrides and further calculate their isochoric vibrational heat capacity $C_V(T)$ at temperatures up to 1000 K [3]. However, the accuracy of the obtained $C_V(T)$ dependences has not yet been assessed, especially at elevated temperatures, which are most important for applications. The high accuracy of the $C_V(T)$ dependences obtained from similar INS measurements has previously been proved only for two hydrides: AlH_3 [4] and MgH_2 [5]. Both hydrides are dielectrics and their $g(E)$ spectra are well reproduced by first-principles calculations. In contrast, the high-pressure hydrides of *d*-elements are all metals, and the electronic contribution to their heat capacity is significant and cannot be accurately calculated. In addition, the accuracy of calculating the optical parts of phonon spectra for metallic hydrides is much worse than for dielectric ones.

Since most high-pressure hydrides of *d*-metals can only be synthesized in rather limited quantities (tens or hundreds of milligrams at best) and are thermally unstable under ambient conditions, none of them have been studied calorimetrically so far. In this paper, using a differential scanning calorimeter PerkinElmer DSC-7, we studied samples of chromium hydride and deuteride weighing about 100 mg each. The samples were synthesized at a hydrogen (deuterium) pressure of 7.4 GPa and a temperature of 873 K and then rapidly cooled (quenched) to 100 K before releasing the pressure. The samples obtained in this way were then stored in liquid nitrogen, and the calorimeter allowed them to be placed in the measuring cell without warming above 100 K. The measurements were carried out at temperatures from 120 to 220–240 K. The lower boundary of the temperature range was the technical limit of the calorimeter; heating the samples above 220–240 K was not possible due to their partial decomposition.

We began our calorimetric studies of high-pressure hydrides with *hcp*-CrH since it was one of the most suitable and interesting objects for investigation. Chromium is commonly used for hydrogen storage in

* Corresponding author.
E-mail address: m.kuzovnikov@ed.ac.uk (M.A. Kuzovnikov).

https://doi.org/10.1016/j.ijhydene.2025.02.448
Received 10 December 2024; Received in revised form 27 January 2025; Accepted 28 February 2025
Available online 14 March 2025

Laves-type intermetallic compounds $TiCr_2$ [6] and $ZrCr_2$ [7], and in multicomponent alloys with a *bcc* (body-centered cubic) structure [8]. Some exotic complex ternary hydrides of chromium compounds are formed under high H_2 pressure, *e.g.*, Mg_3CrH_8 with a high hydrogen content [9]. Chromium hydrides with an *hcp* or *fcc* (face-centered cubic) metal lattice and the composition close to CrH can be prepared by cathodic electrodeposition of chromium [10,11]. Alternatively, *hcp*-CrH samples with a minimum concentration of defects can be prepared from metallic Cr and molecular hydrogen at pressures above ~1.8 GPa [12, 13]. This is well below the upper limit of 9–12 GPa for large-volume high-pressure chambers and allows the synthesis of samples large enough for calorimetric studies (higher chromium hydrides, Cr_2H_3 and CrH_2, are formed at much higher hydrogen pressures of ~17 and ~28 GPa, respectively [14]). Unlike the non-stoichiometric hydrides formed by many *d*-metals [3], chromium hydride has the composition CrH, which simplifies the processing of experimental results and other calculations and makes them more rigorous. The electronic heat capacity coefficient γ_{el} of *hcp*-CrH has previously been determined experimentally [15,16]. The temperature dependences of the molar volume V, coefficient of thermal expansion $\alpha_V = (1/V)(\partial V/\partial T)_P$, and bulk modulus B_0 of *hcp*-CrH have been predicted by *ab initio* calculations [17]. Adding the electronic contribution $C_{el} = \gamma_{el} \cdot T$ and the difference $\Delta C_{PV} = \alpha_V^2 TVB_0$ [18] to the $C_V(T)$ dependence obtained from the INS measurements gave us the isobaric heat capacity $C_P(T)$.

The $C_P(T)$ dependence calculated in this way agrees well with our experimental $C_P(T)$ results, so we used it to calculate the standard (at P = 1 atm) Gibbs energy $G^0_{CrH}(T)$ of the hydride and to determine the temperature dependence of the standard Gibbs energy $\Delta G^0_{eq}(T)$ for the phase equilibrium Cr + (1/2)H_2═CrH. Due to the very large difference in the experimental pressures of formation and decomposition of *hcp*-CrH [13,14,17,19–21] (see Fig. 1), the use of the equilibrium $\Delta G^0_{eq}(T)$ dependence gave a semi-quantitative estimate of the position of the line of phase equilibrium, which lies between the curves of hydride formation and decomposition. To the best of our knowledge, such an assessment has never been carried out for any metal-hydrogen system.

The calorimetric study of chromium hydride was supplemented by a study of chromium deuteride. The main objective of the study was to estimate the ratio E_H/E_D of the energies of optical vibrations of H and D atoms in these compounds and to find out whether it is close to the harmonic value of $\sqrt{m_D/m_H} \approx \sqrt{2} \approx 1.41$, where m_H and m_D are the masses of H and D atoms, or whether it is as large as $E_H/E_D \approx 1.5$ in palladium hydride and deuteride. The problem is that the anomalously large E_H/E_D ratio in the Pd–H/D system, discovered long ago [22], has not yet received a convincing explanation: for many years it was thought to be due to strong anharmonicity of optical vibrations, until later INS studies showed that these vibrations are almost harmonic in both PdH and PdD (see Ref. [23] for discussion and references).

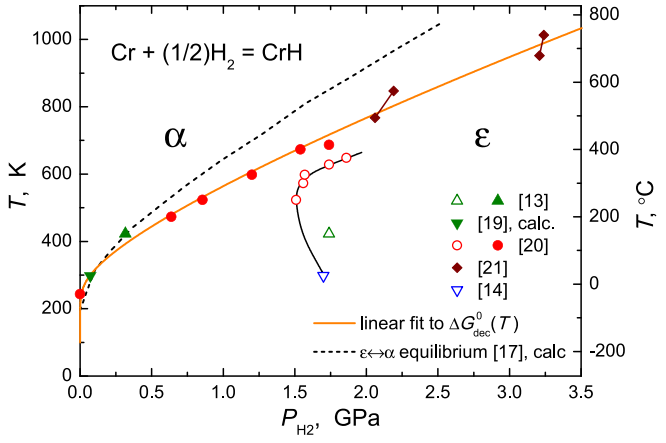

Fig. 1. *T-P* phase diagram of the Cr–H system. The fields of dilute solid hydrogen solutions in Cr and of the *hcp*-CrH hydride are designated as α and ε, respectively. The open symbols indicate the onset of the α→ε transition (hydride formation) at increasing hydrogen pressure or decreasing temperature. The filled symbols stand for the onset of the reverse ε→α transition (hydride decomposition) at decreasing pressure or increasing temperature. The dashed black curve [17] and the point at 0.071 GPa and 298 K [19] represent theoretical estimates for the phase equilibrium Cr + (1/2)H_2═CrH. All other data points are experimental. The solid orange curve is a result of a linear approximation of the $\Delta G^0_{dec}(T)$ dependence for the experimental points of the ε→α transition (see Section 3.3). (For interpretation of the references to color in this figure legend, the reader is referred to the Web version of this article.)

2. Details of experiments and calculations

The starting material was single-crystalline *bcc* chromium metal with a purity of 99.999%. Sample plates were cut from a Cr ingot by spark machining. The damaged surface layer ~0.05 mm was ground off, and then a layer ~0.03 mm was removed by electropolishing in sulfuric acid. The final thickness of the plates was 0.3 mm. The samples intended for hydrogenation (deuteration) were stacks of discs about 7 mm in diameter cut from the plates, each stack weighing about150 mg. The *hcp* monohydride and monodeuteride of chromium were prepared by exposing the Cr samples to an atmosphere of molecular hydrogen (deuterium) at 7.4(3) GPa and 873(15) K for 25 min in a Toroid-type high-pressure chamber [24], using amminoborane NH_3BH_3 and aluminum trideuteride, respectively, as an internal hydrogen (deuterium) source. After the hydrogenation (deuteration) was completed, the sample was quickly cooled (quenched) together with the chamber to ~100 K; the pressure was released; the chamber was disassembled under liquid nitrogen; the sample was removed from the chamber and further stored in liquid nitrogen to prevent hydrogen (deuterium) losses. More details about the method can be found in Ref. [25].

The hydrogen (deuterium) content of the samples was determined with a relative accuracy of 3% by thermal desorption of hydrogen into a pre-evacuated measuring system in the regime of heating from 85 to 920 K at a rate of 10 K/min. The method is described in more detail elsewhere [26]. The mass of the analyzed probe was a few milligrams. Within the experimental error, the obtained samples had stoichiometric compositions of CrH and CrD. As seen from Fig. 2, most of the hydrogen (deuterium) was released from the samples above room temperature. At the same time, the slow release of gas began already at temperatures of

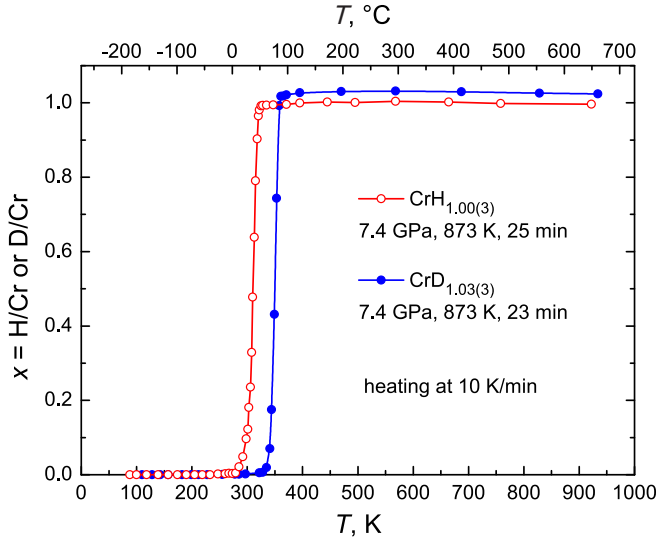

Fig. 2. Temperature dependences of the amount of hydrogen (deuterium) released from quenched *hcp*-CrH and *hcp*-CrD samples heated at 10 K/min in a closed pre-evacuated measuring system.

about 250–270 K, which limited the range of our calorimetric measurements to temperatures of up to 220–240 K.

The samples of hydrogenated and deuterated chromium were examined by X-ray diffraction at 85 K with a powder Siemens D500 diffractometer using Cu Kα radiation selected by a diffracted beam monochromator. The diffractometer was equipped with a home-designed nitrogen cryostat that permitted loading the samples from a liquid N_2 bath without intermediate warming. Prior to the X-ray investigation, each sample was additionally ground in an agate mortar under liquid nitrogen to reduce texture effects. The obtained diffraction patterns were analyzed by the Rietveld profile refinement method using POWDERCELL2.4 software [27]. X-ray diffraction showed that the samples were single-phase *hcp* hydride CrH with lattice parameters at $T = 85$ K $a = 2.718(2)$ Å, $c = 4.426(3)$ Å, $c/a = 1.628(2)$ and deuteride CrD with $a = 2.713(2)$ Å, $c = 4.417(3)$ Å, $c/a = 1.628(2)$, which is consistent with the literature data [10,28,29].

The heat capacity of the CrH and CrD samples was measured with a 5% accuracy at temperatures from 120 to 220–240 K using a PerkinElmer DSC-7 differential scanning calorimeter. The measurements were carried out in the regime of heating at a rate of 20 K/min. The masses of the CrH and CrD samples were 72.0 and 115.2 mg, respectively. The heating rate of 20 K/min was chosen because the heat capacity of these samples measured at 10 and 5 K/min in preliminary experiments was the same, but the $C_P(T)$ dependences appeared significantly noisier. To ensure a good thermal contact with the sample holder, the samples were enclosed into thin aluminum capsules and compacted under a pressure of 0.5 GPa into flat disks 6.6 mm in diameter and 0.4–0.6 mm thick.

The dependence $C_V(T)$ of the isochoric heat capacity of *hcp*-CrH at temperatures up to 1000 K was previously calculated in Ref. [3] using the phonon density of states $g(E)$ derived from INS measurements [30,31]. However, the accuracy of the acoustic part of the $g(E)$ was questionable because the *hcp*-CrH sample studied by INS [31] was prepared by cathodic electrodeposition of chromium and contained many unidentified defects. For this reason, we took a different approach presently and used the acoustic part of $g(E)$ calculated for *hcp*-CrH and *hcp*-CrD with the density-functional theory (DFT).

DFT calculations were performed with the CASTEP code [32] using the Perdew-Burke-Ernzerhof (PBE) exchange-correlation functional [33]. Geometry optimization of the *hcp*-CrH crystal structure was carried out using ultrasoft pseudopotentials generated by CASTEP on-the-fly. A plane-wave basis set with a cutoff energy of 400 eV and a 11x11x6 k-point grid sampling of the Brillouin zone was used for the calculation of electronic properties. The optimized values of the lattice parameters of *hcp*-CrH were $a = 2.675$ Å and $c = 4.352$ Å, which are by about 1.6% smaller than the experimental values. Vibrational properties were calculated with the finite displacement approach using a $4 \times 4 \times 2$ supercell of the original *hcp* unit cell.

3. Results and discussion

3.1. Heat capacity of hcp-CrH

Fig. 3 shows the experimental temperature dependences of the heat capacity $C_P(T)$ for *bcc*-Cr (dashed black curve) borrowed from the literature [34,35] and $C_P^{exp}(T)$ for our CrH sample (segments of thick solid colored curves). To minimize the effects of a gradual baseline shift, the C_P^{exp} dependence for the CrH sample was composed of segments measured in overlapping temperature intervals with a width of 30–40 K. The dashed orange curve starting at 153 K reflects the initial transient process, which was characteristic of each measurement and continued for 10–15 K. The colored segments in Fig. 3 show the valid calorimetric results obtained at temperatures above these transient intervals. To improve the statistical accuracy, the sample was measured at least 3 times in each temperature interval, and the results were averaged.

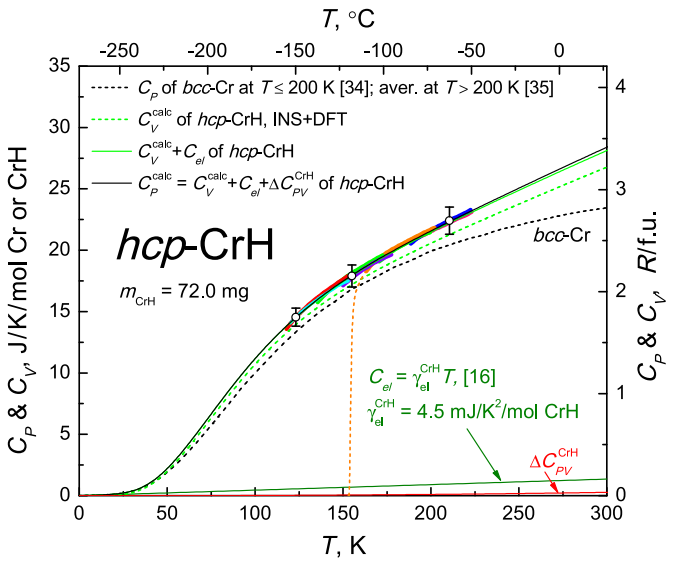

Fig. 3. Experimental temperature dependences of the isobaric heat capacity C_P^{exp} of chromium monohydride *hcp*-CrH measured in this paper at a heating rate of 20 K/min (segments of thick colored curves) and $C_P(T)$ of *bcc*-Cr reported in Refs. [34,35] (dashed black curve). Some experimental points of C_P^{exp} are shown as open black circles intersected by vertical bars, which indicate the experimental error of 5% of the PerkinElmer DSC 7 scanning calorimeter used in the present study. The black solid curve shows the heat capacity of *hcp*-CrH calculated in this paper as $C_P^{calc}(T) = C_V^{calc}(T) + C_{el} + \Delta C_{PV}^{CrH}$, where $C_V^{calc}(T)$ and C_{el} (T) are the phonon and electronic contributions to the heat capacity of *hcp*-CrH, respectively, and ΔC_{PV}^{CrH} is the difference $C_P(T) - C_V(T)$. The C_{el} (T) and $\Delta C_{PV}^{CrH}(T)$ dependences are also presented separately by the olive and red curves, respectively, at the bottom of Figure. $R = 8.314$ J/mol/K is the universal gas constant. The temperature dependences of C_P and C_V for CrH can also be found in digital format in the Supplementary file "Cp and Cv for CrH and CrD.dat", and ΔC_{PV}^{CrH} in the file "Delta Cpv for CrH.DAT". (For interpretation of the references to color in this figure legend, the reader is referred to the Web version of this article.)

As seen from Fig. 3, the experimental dependence $C_P^{exp}(T)$ for CrH is in good agreement with the dependence shown by the black solid curve and calculated as the sum $C_P^{calc}(T) = C_V^{calc}(T) + C_{el} + \Delta C_{PV}^{CrH}$. In this equation, the $C_V^{calc}(T)$ dependence (dashed green curve) is calculated using a combination of the density g_{opt} of optical phonon states derived from INS data [30] and the density g_{ac} of acoustical phonon states calculated with DFT in the present paper. The solid green curve represents the sum of $C_V^{calc}(T)$ and $C_{el}(T) = \gamma_{el} \cdot T$, where the experimental coefficient $\gamma_{el} \cdot = 4.5$ mJ/K^2/mol CrH is taken from Ref. [16]; the electronic contribution $C_{el}(T)$ is also shown separately by the solid olive line at the bottom of Fig. 3. The solid red curve at the bottom of Fig. 3 shows the difference $\Delta C_{PV}^{CrH} = C_P(T) - C_V(T) = \alpha_V^2 TVB_0$ [18] estimated using the temperature dependences of the molar volume V, coefficient of thermal expansion α_V, and bulk modulus B_0 recently predicted for *hcp*-CrH by *ab initio* calculations [17].

Despite the moderate accuracy of calorimetric measurements, their results allow us to judge with confidence that the data used above for calculating the heat capacity of chromium hydride are the most accurate. The main problem with the previous studies of *hcp*-CrH is that almost all of them were carried out on the samples prepared by cathodic electrodeposition of chromium (the method is described, e.g., in Refs. [36,37]) and contained a lot of poorly identified impurities and other defects. As a result, the acoustic part of the INS spectrum of such a sample (solid red circles in Fig. 4) considerably differs from the spectra of all other hydrides of *d*-metals studied so far. In particular, it shows noticeable scattering intensity at $E > 40$ meV between the bands of acoustic and optical vibrations. The cathodic electrodeposition can also

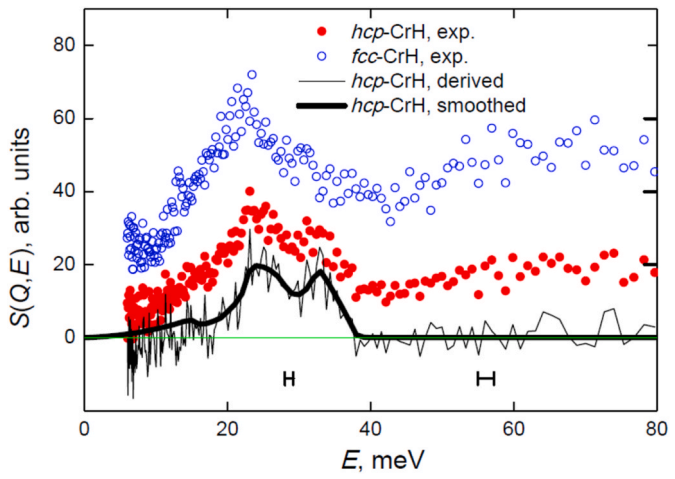

Fig. 4. The dynamical structure factor $S(Q,E)$ of the *hcp*-CrH (solid red circles) and *fcc*-CrH (open blue circles) powder samples at $T = 10$ K as a function of the energy loss E of the inelastically scattered neutrons [31]. Q is the neutron momentum transfer. The horizontal bars indicate the energy resolution. The thick solid curve shows the acoustic part of the spectrum used to calculate the density $g_{ac}(E)$ of acoustic phonons in Ref. [3]. (For interpretation of the references to color in this figure legend, the reader is referred to the Web version of this article.)

produce chromium hydride with a face-centered cubic metal lattice, and a comparative analysis of INS spectra of *hcp*-CrH and *fcc*-CrH (open blue circles in Fig. 4) [31] gave the spectrum of a defect-free *hcp*-CrH plotted with a thin black curve. This spectrum was smoothed (thick black curve in Fig. 4) and further used to calculate $g_{ac}(E)$ [3].

The dashed black curve in Fig. 5 shows $g(E)$ for *hcp*-CrH adopted in Ref. [3]. The optical part of this spectrum was obtained for a sample prepared by reacting chromium metal with gaseous hydrogen at 2 GPa and 600 K, so this sample had the minimum possible number of defects. The accuracy of the acoustical part of $g(E)$ is doubtful. As seen from Fig. 5, it noticeably differs from $g_{ac}(E)$, calculated in this paper and plotted with the red curve.

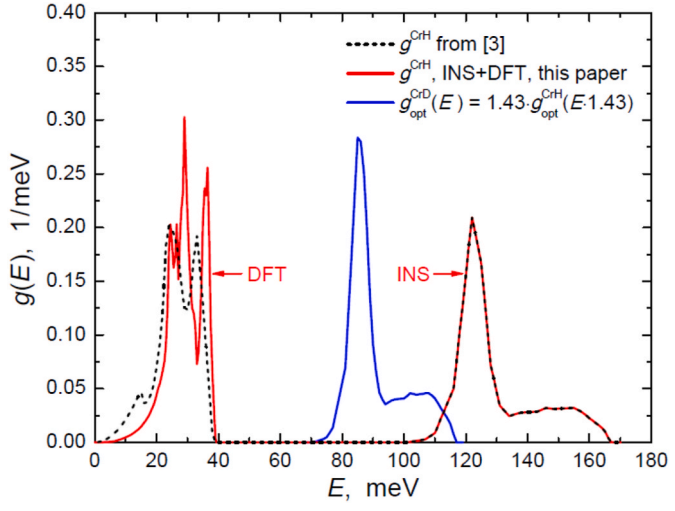

Fig. 5. Phonon densities of states $g(E)$ for *hcp*-CrH and *hcp*-CrD. The dashed black curve represents the spectrum from Ref. [3] and consists of the optical part $g_{opt}(E)$ at $E > 90$ meV measured at $T = 15$ K on the sample synthesized under a high hydrogen pressure, and of the acoustic part $g_{ac}^{depos}(E)$ at $E < 40$ meV calculated from $S(Q,E)$ shown in Fig. 4 by the thick black curve and constructed for the sample prepared by electrodeposition. The red solid curve shows the spectrum for *hcp*-CrH composed of $g_{opt}(E)$ from Ref. [3] and $g_{ac}^{DFT}(E)$ calculated in this paper. The solid blue curve depicts $g_{opt}^{CrD}(E)$ for *hcp*-CrD calculated as $1.43 g_{opt}^{CrH}(E \cdot 1.43)$. The areas under the $g_{ac}(E)$ and $g_{opt}(E)$ curves are set equal to 3 phonon modes each. The spectra $g(E)$ for CrH and CrD can also be found in digital format in the Supplementary file "g(E) of CrH and CrD.dat". (For interpretation of the references to color in this figure legend, the reader is referred to the Web version of this article.)

The spectra $g_{ac}(E)$ and $g_{opt}(T)$ shown in Fig. 5 were used to calculate the temperature dependence of the isochoric heat capacity of *hcp*-CrH and contributions to it from the acoustic and optical phonon bands. Fig. 6 demonstrates these dependences calculated as:

$$C_V(T) = R \cdot \int \left(\frac{E}{k_B T}\right)^2 g(E) n(E,T)[n(E,T)+1]\, dE, \quad (1)$$

where $k_B = 1.381 \cdot 10^{-23}$ J/K is the Boltzmann constant and $n(E,T) = [\exp(E/k_B T) - 1]^{-1}$ is the Bose factor. With the phonon spectra normalized to 6 states in total, this equation gives $C_V(T) \overset{T}{\longrightarrow} \infty 6R = 3R \times 2$ per mole of CrH in accordance with the Dulong and Petit law.

As seen from Fig. 6, the contribution "$C_V^{ac,depos}$ of CrH" from the acoustic vibrations in the *hcp*-CrH sample prepared by cathodic electrodeposition (solid black curve) noticeably differs from "C_V^{ac} of CrH" resulted from the present DFT calculations (magenta curve). The dependence $C_P^{calc,depos}(T)$ calculated using the term "$C_V^{ac,depos}$ of CrH" instead of "C_V^{ac} of CrH" is shown in Fig. 7 with a solid violet curve. This dependence systematically deviates from the experimental one (segments of thick colored curves) as the temperature decreases, and the deviation cannot be compensated for by any means. Therefore, the $g_{ac}^{calc}(E)$ spectrum calculated in this paper (solid red curve in Fig. 5) better represents the density of acoustic phonons in *hcp*-CrH than the $g_{ac}^{depos}(E)$ spectrum shown by the dashed black curve and derived [3] from the INS data for the electrodeposited sample [31].

The hydride *hcp*-CrH is a paramagnetic metal [31,36], and along with phonons, electrons also make a significant contribution to its heat capacity (see Fig. 3). The electronic heat capacity coefficient γ_{el} of *hcp*-CrH was previously determined from low-temperature calorimetric measurements [15,16] on the samples prepared by electrochemical methods. As one can see from Fig. 7, using $\gamma_{el} = 4.5$ mJ/K^2/mol CrH from Ref. [16] provides a good agreement with experiment (see the solid black curve), whereas $\gamma_{el} = 10.25$ mJ/K^2/mol CrH [15] leads to a

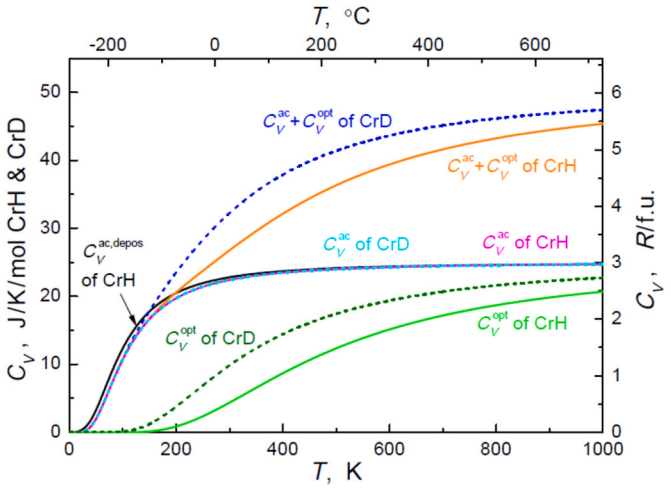

Fig. 6. Temperature dependences of the isochoric heat capacity C_V for *hcp*-CrH (solid curves) and *hcp*-CrD (dashed curves) calculated from the density $g_{ac}(E)$, $g_{opt}(E)$, and $g_{ac}(E) + g_{opt}(E)$ of phonon states proposed in this paper. The solid black curve labeled "$C_V^{ac,depos}$ of CrH" is from Ref. [3]. The $C_V(T)$ dependences for CrD and CrH can also be found in digital format in the Supplementary file "Cp and Cv for CrH and CrD.dat".

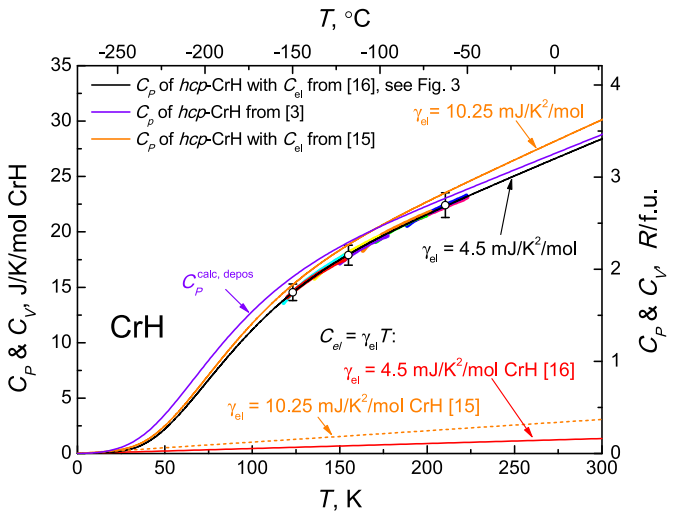

Fig. 7. Temperature dependences of the isobaric heat capacity C_P for *hcp*-CrH. Both the calorimetric results (thick colored sections of the curve) and the most reliable calculated dependence (solid black curve) are taken from Fig. 3. The solid violet curve shows the heat capacity calculated in Ref. [3] using $g(E)$ for the electrodeposited sample (dashed black curve in Fig. 5). The solid orange curve is calculated assuming the electronic heat capacity coefficient $\gamma_{el} = 10.25$ mJ/K^2/mol CrH [15] instead of $\gamma_{el} = 4.5$ mJ/K^2/mol CrH [16] used in this work to calculate the solid black curve. The electronic contributions $C_{el} = \gamma_{el} \cdot T$ with these values of γ_{el} are also shown separately with the dashed orange and solid red lines, respectively, at the bottom of the Figure. (For interpretation of the references to color in this figure legend, the reader is referred to the Web version of this article.)

systematic deviation of the calculated $C_P(T)$ dependence (solid orange curve) with increasing temperature.

The value of $\gamma_{el} = 4.5$ mJ/K^2/mol CrH is also consistent with the results of *ab initio* calculations of the density N_{el} of electronic states. For example, the DFT calculations of this paper yielded the $N_{el}(E_{el})$ dependence (see Fig. S1 in the Supplementary Material) with $N_{el}(E_F) = 0.98$ states/eV/atom Cr at the Fermi energy E_F. In the free electron model, this corresponds to $\gamma_{el} = \left(\pi^2 k_B^2/3\right) N^{el}(E_F) = 2.3$ mJ/K^2/mol CrH. This is half the experimental value of γ_{el} [16], and such a proportion is typical of *d*-metals (see, e.g., Ref. [38]).

We must admit that the reasonable value of γ_{el} determined in Ref. [16] is rather surprising. In fact, the lattice heat capacity coefficient $\beta = 0.042$ mJ/K^4/mol CrH for the low-temperature dependence $C_P = \beta T^3$, which was also determined in that paper, proved to be 16 times higher than $\beta = 0.0026$ mJ/K^4/mol CrH obtained from the $C_V(T)$ dependence calculated in our paper (see Fig. S2 in the Supplementary Material). Most likely, the β value of the chromium hydride sample measured in Ref. [16] significantly exceeded the intrinsic β coefficient of *hcp*-CrH due to the high concentration of defects formed during the electrochemical hydrogenation process. The defects have not yet been identified, but their presence is evidenced, in particular, by the high parasitic intensity in the INS spectrum at energies below the optical phonon band (solid red circles in Fig. 4).

The difference $\Delta C_{PV} = C_P - C_V$ for *hcp*-CrH (solid red curves at the bottom of Fig. 3 and also in Fig. 8c on a larger scale) was determined using the temperature dependences of the coefficient of thermal expansion α_V, molar volume V, and bulk modulus B_0 calculated in Ref. [17]. To improve the accuracy of the theoretical predictions [17], the calculated dependences of these parameters were adjusted to match the available experimental data. The adjusted dependences are plotted in Fig. 8 as hatched curves.

The $\alpha_V(T)$ dependence for *hcp*-CrH was only calculated in Ref. [17] at temperatures above ≈90 K. To construct this dependence at lower temperatures, we used one of Grüneisen's semi-empirical laws to say

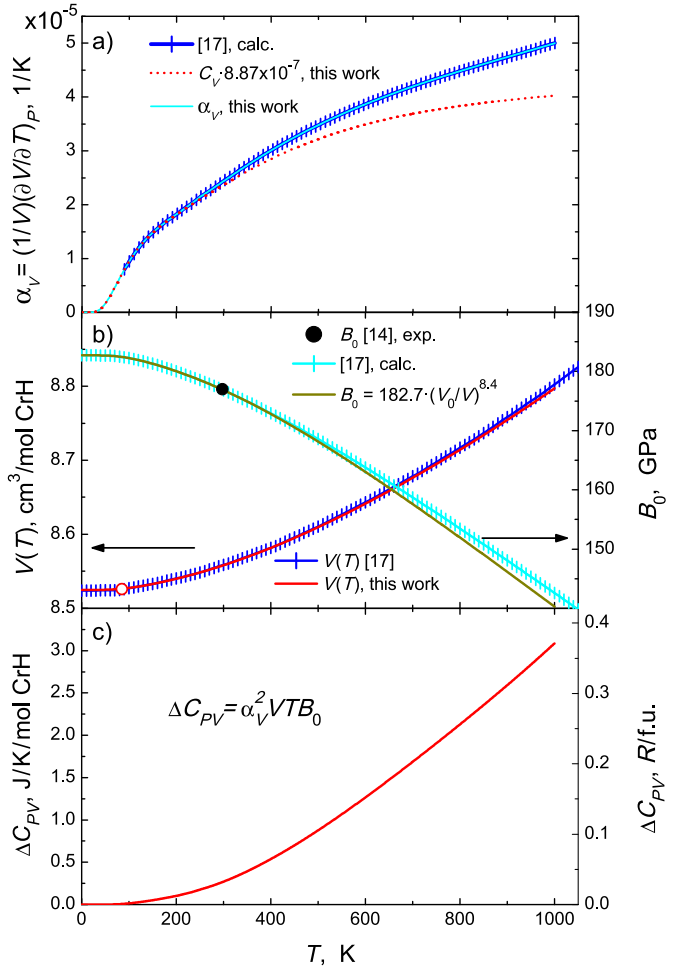

Fig. 8. Temperature dependences of the coefficient of thermal expansion α_V (a); molar volume V (b); bulk modulus B_0 (b), and difference $\Delta C_{PV} = C_P - C_V$ (c) for *hcp*-CrH. The hatched curves show the results of *ab initio* calculations [17]. The dashed red curve in Figure (a) represent the rescaled dependence $C_V(T)$ determined in this paper. The solid dark yellow curve in Figure (b) shows the $B_0(T)$ dependence derived from the Grüneisen relation $B_0(T)/B_0(0\ K) \approx [V(0\ K)/V(T)]^{8.4}$. The dependences shown in this Figure as solid curves can also be found in digital format in the Supplementary file "Delta Cpv for CrH.DAT". (For interpretation of the references to color in this figure legend, the reader is referred to the Web version of this article.)

that $\alpha(T) \approx A \cdot C_V(T)$ (see Ref. [18]). As one can see from Fig. 8a, the choice of the constant $A = 8.87 \cdot 10^{-7}$ (J/mol CrH)$^{-1}$ gives the dependence $\alpha(T)$ (dashed red curve), which smoothly turns into the calculated dependence $\alpha(T)$ (hatched blue curve) at $T > 90$ K. For further estimates, we used $\alpha(T)$ shown in Fig. 8a as a solid cyan curve and consisting of the rescaled $C_V(T)$ at $T \leq 200$ K and $\alpha(T)$ from Ref. [17] at higher temperatures.

Two almost coinciding curves $V(T)$ in Fig. 8b are drawn through the experimental point $V(85\ K) = 8.524$ cm^3/mol CrH (open red circle) obtained by X-ray diffraction in this paper. The hatched blue curve is taken from Ref. [17] and the solid red curve is obtained by integrating the $\alpha(T)$ dependence shown in Fig. 8a with the solid cyan curve.

The hatched cyan curve $B_0(T)$ in Fig. 8b is copied from Ref. [17], where it was drawn through the experimental point $B_0(298\ K) = 177$ GPa [14] shown as a solid black circle. There is a semi-empirical Grüneisen relation stating that $B_0(T) \approx B_0(0\ K)\ [V(0\ K)/V(T)]^{8.4}$ (see Ref. [39] for discussion and references).

As one can see, such a dependence depicted in Fig. 8b with a dark yellow curve well reproduces the dependence calculated in Ref. [17].

The resulting term $\Delta C_{PV} = \alpha_V^2 TVB_0$ presented in Fig. 8c is negligibly

small compared to C_P in the temperature range 120–240 K examined by calorimetry in this paper. Accordingly, the difference between C_P and C_V in this temperature range is determined mainly by the electronic heat capacity, so the good agreement of the experimental C_P and the calculated $C_V + C_{el}$ (see Fig. 3) confirms the validity of $\gamma_{el} = 4.5$ mJ/K^2/mol CrH measured in Ref. [16].

3.2. Heat capacity of hcp-CrD

The temperature dependence of the heat capacity $C_P^{exp}(T)$ of the *hcp*-CrD sample measured in this paper is plotted in Fig. 9 by segments of thick solid colored curves. This experimental dependence is in good agreement with the dark blue curve calculated as $C_P^{calc}(T) = C_V^{calc} + C_{el}^{CrH} + \Delta C_{PV}^{CrH}$. In this equation, we used the $C_{el}^{CrH}(T)$ and $\Delta C_{PV}^{CrH}(T)$ dependences obtained for *hcp*-CrH, since the corresponding dependences for *hcp*-CrD are not yet known. The $C_V^{calc}(T)$ dependence was calculated for *hcp*-CrD using Eq. (1) and $g(E) = g_{ac}^{CrD}(E) + g_{opt}^{CrD}(E)$, where the acoustic $g_{ac}^{CrD}(E)$ was calculated by DFT in this paper and the optical $g_{opt}^{CrD}(E)$ was obtained as $g_{opt}^{CrD}(E) = 1.43 g_{opt}^{CrH}(E \cdot 1.43)$ by rescaling $g_{opt}^{CrH}(E)$ derived from the experimental INS spectrum of *hcp*-CrH [3]. The optical $g_{opt}^{CrD}(E)$ is shown in Fig. 5 by the solid blue curve, while the $g_{ac}^{CrD}(E)$ located at $E < 40$ meV is not shown, because it coincides with the density of acoustic phonons in *hcp*-CrH (solid red curve in Fig. 5) within the line thickness.

The contribution $C_V^{ac}(T)$ of acoustic phonons in *hcp*-CrD almost coincides with $C_V^{ac}(T)$ in *hcp*-CrH as well (compare the curves "C_V^{ac} of CrD" and "C_V^{ac} of CrH" in Fig. 6), and the difference between the $C_P^{calc}(T)$ of *hcp*-CrD and *hcp*-CrH is fully determined by the difference in their $C_V^{opt}(T)$ dependences. As one can see from Fig. 6, in the temperature range 120–240 K of the calorimetric study, the difference is rather large and allows a rough estimate of the coefficient $\eta = E_H/E_D$ of the conversion used to obtain $g_{opt}^{CrD}(E)$, where E_H and E_D are the energies of optical vibrations of CrH and CrD, respectively.

The coefficient $\eta = E_H/E_D$ was previously determined experimentally for hydrides and deuterides of many different metals (a summary of the results can be found in Ref. [3]). As for the monohydrides of *d*-metals of groups VI–X, in which hydrogen atoms occupy octahedral interstices in the close-packed metal lattice, the values $\eta = 1.43$–$1.44 \approx \sqrt{2}$ were found for *fcc* NiH/NiD [40] and *hcp* $MoH_{1.1}/MoD_{1.1}$ [23], and an anomalously large value $\eta = 1.49$–1.51 was obtained for *fcc* PdH/PdD [22,41]. The origin of $\eta \approx 1.5$ for the hydride and deuteride of palladium is not yet clear (see discussion in Ref. [3]), so it cannot be said whether these substances are unique in this respect or not.

In Fig. 10, the solid cyan curve depicts the $C_P^{calc}(T)$ dependence calculated using $g_{opt}^{CrD}(E) = 1.51 g_{opt}^{CrH}(E \cdot 1.51)$, while the other parameters remained unchanged. The curve systematically deviates upward from the experimental C_P^{exp} dependence as the temperature increases. This indicates that the value of η should be lower than 1.51, and using the value $\eta = 1.43$ experimentally determined for the pairs NiH/NiD [40] and $MoH_{1.1}/MoD_{1.1}$ [23] appears more appropriate (see the dark blue curve).

Regretfully, the aluminum trideuteride used as the source of deuterium in the synthesis of the *hcp*-CrD sample was contaminated with 3 at. % H. Consequently, the sample must also have been contaminated with protium. When we used the same trideuteride for a high-pressure synthesis of deuterides of palladium [41] and molybdenum [23], the obtained samples contained about 5 and 7 at.% H, respectively. The protium content of the *hcp*-CrD sample studied in this work was not determined experimentally. To estimate from above the effect of the protium impurity on the heat capacity of this sample, the solid orange curve in Fig. 10 shows a $C_P(T)$ dependence for a sample consisting of 90% CrD and 10% CrH. As one can see, the effect is small in the studied temperature interval below 240 K and it cannot annul the conclusion that $\eta = 1.51$ is too large for the CrH/CrD pair.

Having made sure that the $C_P^{calc}(T)$ dependences calculated on the basis of the INS data well described the experimental $C_P^{exp}(T)$ dependences of *hcp*-CrH and *hcp*-CrD at temperatures up to 240 K, we extended the $C_P^{calc}(T)$ dependences to 1000 K (see Fig. 11).

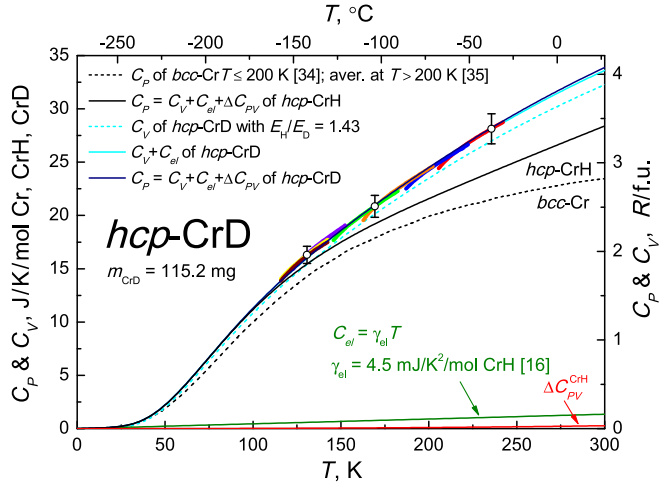

Fig. 9. Segments of thick colored curves represent the temperature dependence of the isobaric heat capacity C_P^{exp} of *hcp*-CrD measured at a heating rate of 20 K/min. Some experimental points of C_P^{exp} are plotted as open black circles intersected by vertical bars indicating the experimental error 5%. The solid blue curve shows the $C_P^{calc}(T)$ dependence of *hcp*-CrD calculated in this paper as the sum of the phonon heat capacity C_V^{calc} of *hcp*-CrD (dashed cyan curve), the electronic heat capacity C_{el}^{CrH} (solid olive line at the bottom of the Figure) and the difference $\Delta C_{PV}^{CrH} = C_P(T) - C_V(T)$ (solid red curve at the bottom of the Figure). Also shown are the sum $C_V^{calc} + C_{el}^{CrH}$ for *hcp*-CrD (solid cyan curve), C_P^{exp} for *hcp*-CrH (solid black curve), and the experimental C_P for *bcc*-Cr reported in Refs. [34,35] (dashed black curve). The temperature dependences of C_P and C_V for CrD and C_P for CrH can also be found in digital format in the Supplementary file "Cp and Cv for CrH and CrD.dat", and ΔC_{PV}^{CrH} in the file "Delta Cpv for CrH. DAT". (For interpretation of the references to color in this figure legend, the reader is referred to the Web version of this article.)

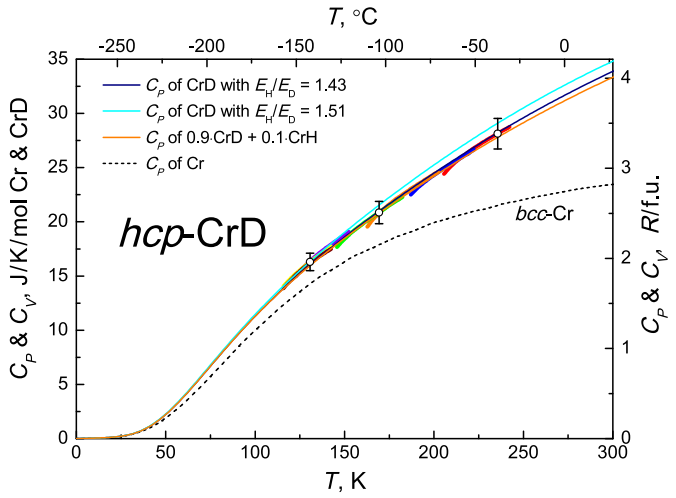

Fig. 10. Temperature dependences of the isobaric heat capacity C_P for *hcp*-CrD and *bcc*-Cr. The solid blue curve is the same as in Fig. 9. The solid cyan curve represents the sum $C_V^{calc} + C_{el}^{CrH} + \Delta C_{PV}^{CrH}$, where C_V^{calc} is calculated using $g_{opt}^{CrD}(E) = 1.51 g_{opt}^{CrH}(E \cdot 1.51)$. The solid orange curve shows the heat capacity of a mixture of 90% CrD +10% CrH. (For interpretation of the references to color in this figure legend, the reader is referred to the Web version of this article.)

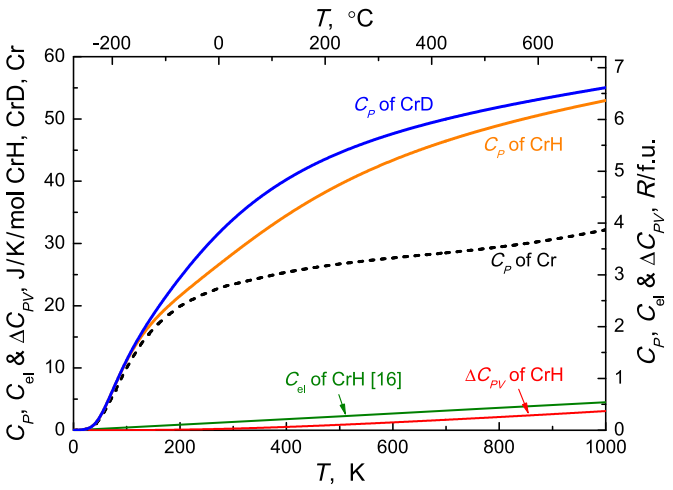

Fig. 11. Temperature dependences of the isobaric heat capacity C_P for *hcp*-CrH (orange curve) and *hcp*-CrD (blue curve) calculated in this paper. The dashed black curve presents the experimental $C_P(T)$ for *bcc*-Cr reported in Refs. [34,35]. The red and olive curves at the bottom of the Figure show, respectively, the difference $\Delta C_{PV}^{CrH} = C_P - C_V$ for *hcp*-CrH calculated in this paper and the electronic heat capacity $C_{el}^{CrH}(T) = \gamma_{el} \cdot T$ with the experimental coefficient $\gamma_{el} = 4.5$ mJ/K^2/mol CrH determined in Ref. [16]. The $C_P(T)$ and $C_V(T)$ dependences for CrD and CrH can also be found in digital format in the Supplementary file "Cp and Cv for CrH and CrD.dat", and ΔC_{PV} of CrH in the file "Delta Cpv for CrH.DAT". (For interpretation of the references to color in this figure legend, the reader is referred to the Web version of this article.)

3.3. T-P phase diagram of the Cr–H system

The $C_P(T)$ dependences shown in Fig. 11 were further used to calculate the standard enthalpy $H^0(T) = \int_0^T C_P(\tau)d\tau$, standard entropy $S^0(T) = \int_0^T [C_P(\tau)/\tau]d\tau$, and standard Gibbs energy $G^0(T) = H^0 - T{\cdot}S^0$ for *hcp*-CrH, *hcp*-CrD, and *bcc*-Cr. The $G^0(T)$ dependences thus obtained are depicted in Fig. 12 together with the $G^0(T)$ dependences for gaseous H_2 and D_2 from the literature. These $G^0(T)$ dependences were further used to calculate the "equilibrium" Gibbs energies $\Delta G^0(T)$ of formation of *hcp*-CrH and *hcp*-CrD shown in the upper part of Fig. 12. As one can see, both $\Delta G^0(T)$ dependences are almost linear, and a linear fit (thin straight lines) gives constant values of $\Delta S^0 = 64.4(1)$ and 66.2(1) J/K/mol for the formation of chromium hydride and deuteride, respectively.

The $\Delta G^0(T)$ dependences calculated in this way cannot give us the enthalpy ΔH^0 of the reaction, since the energies $G^0(T)$ are not measured from the same level. However, in the case of the Cr–H system, we can estimate ΔH^0 by comparing the $\Delta G^0(T)$ curve with the $\Delta G^0_{form}(T)$ and $\Delta G^0_{dec}(T)$ dependences calculated for the available experimental $T(P)$ points of formation and decomposition of *hcp*-CrH (see Fig. 1). For the decomposition we can write:

$$\Delta G^0_{dec}(T) = \int_{P_{dec}}^{P_0} \Delta V dP = \int_{P_{dec}}^{P_0} \left(V_{CrH} - V_{Cr} - \frac{1}{2}V_{H_2}\right) dP \approx -\beta_H P_{dec} + \frac{1}{2}\int_{P_0}^{P_{dec}} V_{H_2} dP. \quad (2)$$

In this equation, $\beta_H = 1.33$ cm^3/mol is the difference between the molar volumes of *hcp*-CrH and *bcc*-Cr under normal conditions and $V_{H_2}(T,P)$ is the molar volume of molecular hydrogen. The equation for $\Delta G^0_{form}(T)$ is similar. The volume $V_{H_2}(T,P)$ was calculated using the equation of state from Ref. [45] at pressures above 1 MPa and the equation for ideal gases at $0.1 \le P \le 1$ MPa. The obtained points $\Delta G^0_{dec}(T)$ and $\Delta G^0_{form}(T)$ are presented in Fig. 13.

As seen from Fig. 13, the $\Delta G^0_{dec}(T)$ points all lie on the linear dependence $\Delta G^0_{dec}(T) = \Delta H^0_{dec} - T{\cdot}\Delta S^0_{dec}$ shown with a solid orange line; the fitting parameters of this line are $\Delta H^0_{dec} = -12.7(7)$ kJ/mol and $\Delta S^0_{dec} = 71.3(10)$ J/K/mol. The $T_{dec}(P_{dec})$ dependence calculated from $\Delta G^0_{dec}(T)$ using Eq. (2) is shown in Fig. 1 and 14 with a solid orange line,

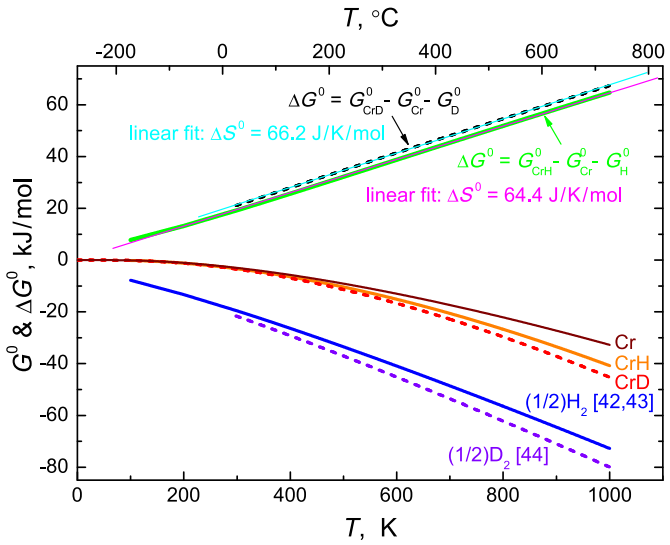

Fig. 12. Temperature dependences of the standard (at $P_0 = 1$ atm) Gibbs energy G^0 of the components of the reactions Cr + (1/2)H_2 → CrH (solid curves) and Cr + (1/2)D_2 → CrD (dashed curves) and of the Gibbs energy ΔG^0 of these reactions (two upper curves). The thin solid straight lines represent linear fits to the ΔG^0(T) dependences. The literature data for gaseous H_2 are taken from Ref. [42] at $T \ge 298$ K and Ref. [43] at $T < 298$ K, and for gaseous D_2 from Ref. [44]. The dependences shown in this Figure for CrH and CrD can also be found in digital format in the Supplementary files "DeltaG0 for CrH.DAT" and "DeltaG0 for CrD.DAT", respectively.

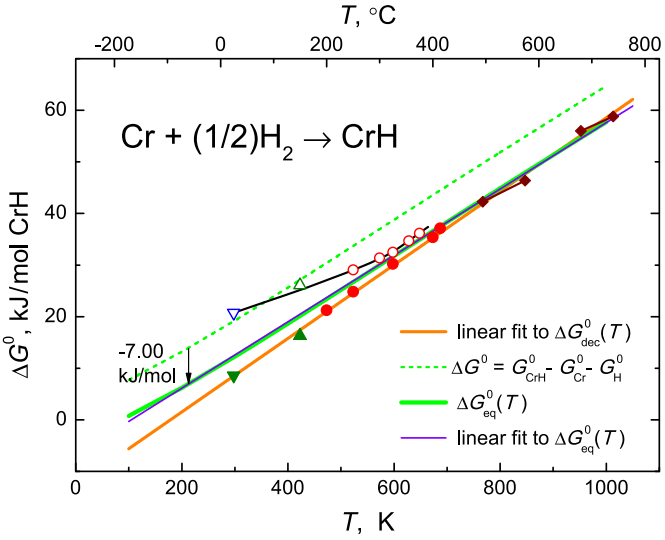

Fig. 13. Standard Gibbs energy $\Delta G^0(T)$ of the Cr + (1/2)H_2 → CrH reaction taken from Fig. 12 (dashed green curve), $\Delta G^0_{dec}(T)$ of decomposition of *hcp*-CrH (solid symbols), and $\Delta G^0_{form}(T)$ of its formation (open symbols). The shape and color of the symbols are the same as in Fig. 1. The solid green curve is obtained by shifting the $\Delta G^0(T)$ curve downwards by 7.00 kJ/mol; this solid curve is further considered as $\Delta G^0_{eq}(T)$ of the Cr + (1/2)H_2═CrH equilibrium. The thin straight lines are linear approximations of the $\Delta G^0_{eq}(T)$ and $\Delta G^0_{dec}(T)$ dependences. The dependence $\Delta G^0_{dec}(T)$ can also be found in digital format in the Supplementary file "Peq and DeltaG0eq for CrH.DAT". (For interpretation of the references to color in this figure legend, the reader is referred to the Web version of this article.)

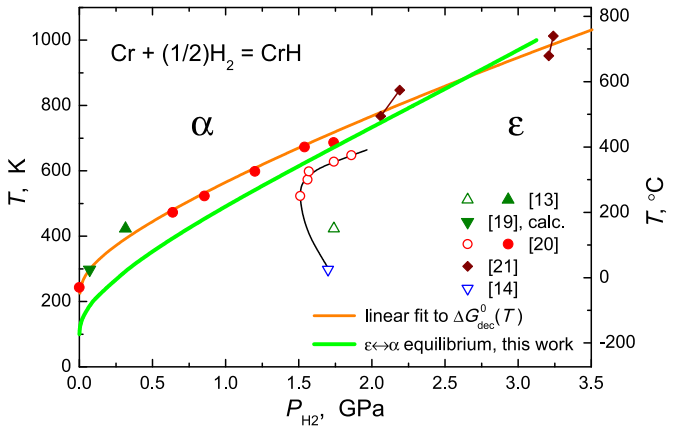

Fig. 14. *T-P* phase diagram of the Cr–H system. The solid green curve shows the line of the Cr + (1/2)H_2═CrH equilibrium calculated from the $\Delta G^0_{eq}(T)$ dependence (solid green curve in Fig. 13) using Eq. (2). Other designations are the same as in Fig. 1. The dependence $P_{eq}(T)$ can also be found in digital format in the Supplementary file "Peq and DeltaG0eq for CrH.DAT". (For interpretation of the references to color in this figure legend, the reader is referred to the Web version of this article.)

too.

The thick solid green curve $T_{eq}(P_{eq})$ in Fig. 14 represents the Cr + (1/2)H_2═CrH equilibrium. It was calculated using an analogue of Eq. (2) and the $\Delta G^0_{eq}(T)$ dependence shown in Fig. 13 with the thick green curve, which was obtained by shifting the $\Delta G^0(T)$ dependence (dashed green curve) downwards by 7.00 kJ/mol. The value of the shift was chosen so that the resulting $T_{eq}(P_{eq})$ curve passed between the curves of formation and decomposition of *hcp*-CrH in the pressure interval 1.5–1.8 GPa, where the distance between them is minimal. At room temperature, $\Delta G^0_{eq}(298\ K) = 12.1$ kJ/mol; $\Delta H^0_{eq}(298\ K) = -6.5$ kJ/mol; $\Delta S^0_{eq}(298\ K) = -62.6$ J/K/mol. The parameters of the linear approximation (straight violet line in Fig. 13) of the $\Delta G^0_{eq}(T)$ dependence have similar values of $\Delta H^0 = -6.74(5)$ kJ/mol and $\Delta S^0 = -64.35(7)$ J/K/mol.

As seen from Fig. 14, the value of P_{eq} (298 K) ≈ 0.33 GPa is approximately 5 times higher than $P_{dec} = 0.071$ GPa [19] and 5 times lower than $P_{form} = 1.7$ GPa [14]. This is consistent with the most common view that in the metal-hydrogen systems, the pressure of thermodynamic equilibrium is usually much closer to the pressure of hydride decomposition than to the pressure of its formation.

4. Conclusions

Despite the moderate accuracy of 5% and limited temperature range, the calorimetric study of chromium hydride and deuteride added quite a lot of information about their physical and thermodynamic properties. In our opinion, the most interesting result is the semi-quantitative localization of the line of the Cr + (1/2)H_2═CrH equilibrium between the curves of hydride formation and decomposition. Based on indirect evidence, the majority of the hydride community has gradually come to the opinion that the equilibrium pressure should be closer to the decomposition pressure of the hydride and may almost coincide with it. The investigation of the Cr–H system provided experimental support for this opinion.

To facilitate further use of the temperature dependences of the heat capacities, Gibbs free energies and other thermodynamic parameters, as well as the curve of the Cr + (1/2)H_2═CrH equilibrium determined in this paper, they are presented in digital form in the Supplementary Information.

CRediT authorship contribution statement

Mikhail A. Kuzovnikov: Writing – review & editing, Writing – original draft, Project administration, Formal analysis. **Vladimir E. Antonov:** Writing – original draft, Investigation, Conceptualization. **Valery I. Kulakov:** Investigation. **Radion I. Usmanov:** Investigation.

Declaration of competing interest

The authors declare that they have no known competing financial interests or personal relationships that could have appeared to influence the work reported in this paper.

Acknowledgments

The work was funded by the Russian Science Foundation under project no. 23-22-00361 and by the Horizon 2020 program of the European Union (Grant no. 948895, MetElOne).

Appendix A. Supplementary data

Supplementary data to this article can be found online at https://doi.org/10.1016/j.ijhydene.2025.02.448.

References

[1] Antonov VE. Phase transformations, crystal and magnetic structures of high-pressure hydrides of d-metals. J Alloys Compd 2002;330–332:110–6. https://doi.org/10.1016/S0925-8388(01)01532-8.
[2] Kuzovnikov MA, Minkov VS, Chariton S, Prakapenka VB, Eremets MI. Synthesis of osmium hydride under high hydrogen pressure. Phys Rev B 2020;102:214109. https://doi.org/10.1103/PhysRevB.102.214109.
[3] Antonov VE, Fedotov VK, Ivanov AS, Kolesnikov AI, Kuzovnikov MA, Tkacz M, Yartys VA. Lattice dynamics of high-pressure hydrides studied by inelastic neutron scattering. J Alloys Compd 2022;905:164208. https://doi.org/10.1016/j.jallcom.2022.164208.
[4] Antonov VE, Kolesnikov AI, Markushkin YE, Palnichenko AV, Ren Y, Sakharov MK. Heat capacity of α-AlH_3 and α-AlD_3 at temperatures up to 1000 K. J Phys Condens Matter 2008;20:275204. https://doi.org/10.1088/0953-8984/20/27/275204.
[5] Kolesnikov AI, Antonov VE, Efimchenko V, Granroth G, Klyamkin SN, Levchenko AV, Sakharov MK, Ren Y. Neutron spectroscopy of magnesium dihydride. J Alloys Compd 2011;509S:S599–603. https://doi.org/10.1016/j.jallcom.2010.10.156.
[6] McGrath AJ, Wadge MD, Adams M, Manickam K, Ling S, Walker GS, Grant DM. Stoichiometry and annealing condition on hydrogen capacity of $TiCr_{2-x}$ AB_2 alloys. Int J Hydrogen Energy 2024;53:582–91. https://doi.org/10.1016/j.ijhydene.2023.12.062.
[7] Dorogova M, Hirata T, Filipek SM, Bala H. Synthesis of a hexagonal hydride phase of $ZrCr_2H_x$ ($x = 5.75$) under high hydrogen pressure. J Phys Condens Matter 2002;14:11151–6. https://doi.org/10.1088/0953-8984/14/44/443.
[8] Okada M, Kuriiwa T, Tamura T, Takamura H, Kamegawa A. Ti–V–Cr b.c.c. alloys with high protium content. J Alloys Compd 2002;330–332:511–6. https://doi.org/10.1016/S0925-8388(01)01647-4.
[9] Takagi S, Iijima Y, Sato T, Saitoh H, Ikeda K, Otomo T, Miwa K, Ikeshoji T, Aoki K, Orimo Shin-ichi. True boundary for the formation of homoleptic transition-metal hydride complexes. Angew Chem Int Ed 2015;54:5650–3. https://doi.org/10.1002/anie.201500792.
[10] Stock AD, Hardcastle KI. Phase and composition analysis of chromium hydride. J Inorg Nucl Chem 1970;32:1183–6. https://doi.org/10.1016/0022-1902(70)80113-0.
[11] Tkacz M. High pressure studies of the FCC chromium hydride. Rev High Pres Sci Technol 1998;7:263–5. https://doi.org/10.4131/jshpreview.7.263.
[12] Baranowski B, Bojarski K. Formation of chromium hydride from metallic chromium and high pressure gaseous hydrogen. Roczn Chem 1972;46:525–7.
[13] Baranowski B. Thermodynamics of metal/hydrogen systems at high pressures. Ber. Bunsenges. phys. Chem. 1972;76:714–24. https://doi.org/10.1002/bbpc.19720760805.
[14] Marizy A, Geneste G, Loubeyre P, Guigue B, Garbarino G. Synthesis of bulk chromium hydrides under pressure of up to 120 GPa. Phys Rev B 2018;97:184103. https://doi.org/10.1103/PhysRevB.97.184103.
[15] Albrecht G, Wolf G. Spezifische Elektronenwärme und λ-Anomalie von $CrH_{0.84}$. Phys Status Solidi 1966;18:K119–22. https://doi.org/10.1515/9783112498149-052.
[16] Viswanathan R, Khan HR, Knoedler A, Raub ChJ. Low-temperature heat capacity of $CrH_{0.97}$. J Appl Phys 1975;46:4088–9. https://doi.org/10.1063/1.322120.
[17] Dottor M, Crivello J-C, Joubert J-M. Thermodynamic modeling of Cr and Cr-H systems up to high temperatures and high pressures. Int J Hydrogen Energy 2022;47:23293–309. https://doi.org/10.1016/j.ijhydene.2022.04.245.

[18] Landau LD, Lifshitz EM. Statistical physics. Part 1, third ed. Oxford: Pergamon; 1980.
[19] Baranowski B, Bojarski K. Free energy of formation of chromium hydride. Roczn Chem 1972;46:1403–9.
[20] Ponyatovskii EG, Belash IT. Formation and decomposition of chromium hydride at temperatures to 400 °C and pressures to 20 kbar. Dokl Akad Nauk SSSR 1976;229:1171–3. in Russian.
[21] Fukai Y, Mizutani M. Phase diagram and superabundant vacancy formation in Cr–H alloys. Mater Trans 2002;43:1079–84. https://doi.org/10.2320/MATERTRANS.43.1079.
[22] Rush JJ, Rowe JM, Richter D. Direct determination of the anharmonic vibrational potential for H in Pd. Z Phys B 1984;55:283–6. https://doi.org/10.1007/BF01304078.
[23] Kuzovnikov MA, Antonov VE, Hansen T, Ivanov AS, Kolesnikov AI, Kulakov VI, Muzalevsky VD, Savvin S, Tkacz M. Isotopic dependence of the frequency of optical vibrations in molybdenum monohydride. J Alloys Compd 2022;893:162299. https://doi.org/10.1016/j.jallcom.2021.162299.
[24] Khvostantsev LG, Slesarev VN, Brazhkin VV. Toroid type high-pressure device: history and prospects. High Press Res 2004;24(3):371–83. https://doi.org/10.1080/08957950412331298761.
[25] Antonov VE, Bulychev BM, Fedotov VK, Kapustin DI, Kulakov VI, Sholin IA. NH_3BH_3 as an internal hydrogen source for high pressure experiments. Int J Hydrogen Energy 2017;42:22454–9. https://doi.org/10.1016/j.ijhydene.2017.03.121.
[26] Bashkin IO, Antonov VE, Bazhenov AV, Bdikin IK, et al. Thermally stable hydrogen compounds obtained under high pressure on the basis of carbon nanotubes and nanofibers. JETP Lett 2004;79(5):226–30. https://doi.org/10.1134/1.1753421.
[27] Kraus W, Nolze GJ. *Powder cell* – a program for the representation and manipulation of crystal structures and calculation of the resulting x-ray powder patterns. J Appl Crystallogr 1996;29(3):301–3. https://doi.org/10.1107/S0021889895014920.
[28] Roy RJ, Gibb TRP. The paramagnetic susceptibility of chromium hydride. J Inorg Nucl Chem 1967;29:341–5. https://doi.org/10.1016/0022-1902(67)80036-8.
[29] Baranowski B, Tkacz M. Formation of chromium deuteride from metallic chromium and high pressure gaseous deuterium. Roczn Chem 1974;48(4):713–4. https://doi.org/10.1002/chin.197431056.
[30] Dorner B, Belash IT, Bokhenkov EL, Ponyatovsky EG, Antonov VE, Pronina LN. Inelastic incoherent neutron scattering spectra from fcc $NiH_{1.05}$, hcp $CrH_{1.0}$ and hcp $MoH_{1.2}$ at 15K. Solid State Commun 1989;69(2):121–4. https://doi.org/10.1016/0038-1098(89)90374-8.
[31] Antonov VE, Beskrovnyy AI, Fedotov VK, Ivanov AS, Khasanov SS, Kolesnikov AI, Sakharov MK, Sashin IL, Tkacz M. Crystal structure and lattice dynamics of chromium hydrides. J Alloys Compd 2007;430:22–8. https://doi.org/10.1016/j.jallcom.2006.05.021.
[32] Clark SJ, Segall MD, Pickard CJ, Hasnip PJ, Probert MJ, Refson K, Payne MC. First principles methods using CASTEP. Z Kristallogr 2005;220:567–70. https://doi.org/10.1524/zkri.220.5.567.65075.
[33] Perdew JP, Burke K, Ernzerhof M. Generalized gradient approximation made simple. Phys Rev Lett 1996;77:3865. https://doi.org/10.1103/PhysRevLett.77.3865.
[34] Clusius K, Franzosini P. Ergebnisse der Tieftemperaturforschung. XXXII. Atom- und Elektronenwarme des Chroms zwischen 14 °K und 273 °K. Z Naturforsch 1962;17(6):522–5.
[35] Touloukian MS, Buyco EH. Specific heat: metallic elements and alloys. In: Thermophysical properties of matter, vol. 4. New York – Washington: IFI/Plenum; 1970. p. 44–7. 0306670240, 9780306670244.
[36] Poźniak-Fabrowska J, Nowak B, Tkacz M. Magnetic properties of cubic and hexagonal chromium hydrides: a comparison of the magnetic susceptibility with the ^{53}Cr NMR Knight shift. J Alloys Compd 2001;322:82–8. https://doi.org/10.1016/S0925-8388(01)01266-X.
[37] Tkacz M. High pressure studies of the FCC chromium hydride. Pol J Chem 1997;71(12):1735–41.
[38] Irkhin VY, Irkhin YP. Electronic structure, physical properties, and correlation effects in *d*- and *f*-metals and their compounds. Moscow–Izhevsk, Izd. Regular and Chaotic Dynamics 2008:476. 978-5-93972-684-9. (in Russian).
[39] Fürth R. On the stability of crystal lattices. Math Proc Camb Phil Soc 1941;37(2):177–85. https://doi.org/10.1017/S0305004100021666.
[40] Antonov VE, Ivanov AS, Kuzovnikov MA, Tkacz M. Neutron spectroscopy of nickel deuteride. J Alloys Compd 2013;580:S109–13. https://doi.org/10.1016/j.jallcom.2013.03.021.
[41] Antonov VE, Davydov AI, Fedotov VK, Ivanov AS, Kolesnikov AI, Kuzovnikov MA. Neutron spectroscopy of H impurities in PdD: covibrations of the H and D atoms. Phys Rev B 2009;80:134302. https://doi.org/10.1103/PhysRevB.80.134302.
[42] NIST Chemistry WebBook. https://webbook.nist.gov/cgi/cbook.cgi?ID=C1333740&Units=SI&Mask=1&Type=JANAFG&Plot=on#JANAFG.
[43] Hemmes H, Driessen A, Griessen R. Thermodynamic properties of hydrogen at pressures up to 1 Mbar and temperatures between 100 and 1000 K. J Phys C Solid State Phys 1986;19:3571–85. https://doi.org/10.1088/0022-3719/19/19/013.
[44] NIST Chemistry WebBook. https://webbook.nist.gov/cgi/cbook.cgi?ID=C7782390&Units=SI&Mask=1&Type=JANAFG&Plot=on#JANAFG.
[45] Tkacz M, Litwiniuk A. Useful equations of state of hydrogen and deuterium. J Alloys Compd 2002;330–332:89–92. https://doi.org/10.1016/S0925-8388(01)01488-8.